# Twofold transition in $\mathcal{PT}$-symmetric coupled oscillators

Carl M. Bender,[1,*] Mariagiovanna Gianfreda,[2,†] Şahin K. Özdemir,[3,‡] Bo Peng,[3,§] and Lan Yang[3,¶]
[1]*Department of Physics, Washington University, St. Louis, Missouri 63130, USA*
[2]*Dipartimento di Matematica e Fisica Ennio De Giorgi, Università del Salento and I. N. F. N. Sezione di Lecce, Via Arnesano, I-73100 Lecce, Italy*
[3]*Electrical and Systems Engineering, Washington University, St. Louis, Missouri 63130, USA*
(Received 21 October 2013; published 26 December 2013)

The inspiration for this theoretical paper comes from recent experiments on a $\mathcal{PT}$-symmetric system of two coupled optical whispering galleries (optical resonators). The optical system can be modeled as a pair of coupled linear oscillators, one with gain and the other with loss. If the coupled oscillators have a balanced loss and gain, the system is described by a Hamiltonian and the energy is conserved. This theoretical model exhibits *two* $\mathcal{PT}$ transitions depending on the size of the coupling parameter $\epsilon$. For small $\epsilon$, the $\mathcal{PT}$ symmetry is broken and the system is not in equilibrium, but when $\epsilon$ becomes sufficiently large, the system undergoes a transition to an equilibrium phase in which the $\mathcal{PT}$ symmetry is unbroken. For very large $\epsilon$, the system undergoes a second transition and is no longer in equilibrium. The principal result presented here is that the classical and quantized versions of the system exhibit transitions at exactly the same values of $\epsilon$.

DOI: 10.1103/PhysRevA.88.062111 PACS number(s): 11.30.Er, 03.65.−w, 02.30.Mv, 11.10.Lm

## I. INTRODUCTION

The predicted properties of $\mathcal{PT}$-symmetric Hamiltonians [1,2] have been observed at the classical level in a wide variety of laboratory experiments involving superconductivity [3,4], optics [5–8], microwave cavities [9], atomic diffusion [10], nuclear magnetic resonance [11], and coupled electronic and mechanical oscillators [12,13]. Although $\mathcal{PT}$-symmetric systems were originally explored at a highly mathematical level, it is now understood that one can interpret $\mathcal{PT}$-symmetric systems simply as nonisolated physical systems having a balanced loss and gain.

In this paper, we examine a mathematical model based on recent experiments [14], which were performed on a system consisting of two coupled $\mathcal{PT}$-symmetric whispering-gallery-mode optical resonators with experimental coupling constant $\kappa$. Such a system is $\mathcal{PT}$-symmetric if one resonator has an optically driven gain and the other resonator has a balanced loss. The experimental setup is shown schematically in Fig. 1. We examine here the properties of the mathematical model on a theoretical level and we study both the classical and the quantum versions of the system.

A system of two identical coupled resonators, one with loss and the other with gain, can be modeled as coupled oscillators whose amplitudes are $x(t)$ and $y(t)$. Both oscillators have a natural frequency $\omega$. The first oscillator $x$ is subject to a friction force $\mu\dot{x}$ ($\mu > 0$), while the second oscillator $y$ is subject to an antifriction force $-\nu\dot{y}$ ($\nu > 0$). The parameters $\mu$ and $\nu$ are a measure of the loss and gain. The oscillators are coupled linearly and the coupling strength is represented by the parameter $\epsilon$. The equations of motion of these oscillators are

$$\ddot{x} + \omega^2 x + \mu\dot{x} = -\epsilon y, \quad \ddot{y} + \omega^2 y - \nu\dot{y} = -\epsilon x. \tag{1}$$

To treat this system at a classical level, we seek solutions to (1) of the form $e^{i\lambda t}$. The frequency $\lambda$ satisfies the quartic polynomial equation

$$\lambda^4 - i(\mu - \nu)\lambda^3 - (2\omega^2 - \mu\nu)\lambda^2 + i\omega^2(\mu - \nu)\lambda - \epsilon^2 + \omega^4 = 0. \tag{2}$$

An important special case arises when the loss and gain are balanced, that is, when $2\gamma = \mu = \nu$. In this case, the frequencies $\lambda$ are the roots of the quartic polynomial $f(\lambda)$, where

$$f(\lambda) = \lambda^4 - (2\omega^2 - 4\gamma^2)\lambda^2 - \epsilon^2 + \omega^4. \tag{3}$$

For this special case, the classical equations of motion (1) can be derived from the Hamiltonian [15]

$$H = pq + \gamma(yq - xp) + (\omega^2 - \gamma^2)xy + \epsilon(x^2 + y^2)/2. \tag{4}$$

If the coupling parameter $\epsilon$ of the $x$ and $y$ oscillators is set to zero, this Hamiltonian reduces to the Hamiltonian considered by Bateman [16]. In his paper, Bateman sought a variational principle to derive an equation of motion having a friction term linear in velocity. To do so, he introduced an additional degree of freedom, namely a time-reversed version of the original damped harmonic oscillator. This auxiliary oscillator acts as an energy reservoir and can be considered as an effective description of a thermal bath. The classical Hamiltonian for the Bateman system was constructed by Morse and Feschbach [17] and the corresponding quantum theory was analyzed by many authors, including Bopp [18], Feshbach and Tikochinsky [19], Tikochinsky [20], Dekker [21], Celeghini, Rasetti, and Vitiello [22], Banerjee and Mukherjee [23], and Chruściński and Jurkowski [24]. We emphasize that in all these references, only the *noninteracting* ($\epsilon = 0$) case was considered. It is easy to see that the Hamiltonian (4) is $\mathcal{PT}$-symmetric, where the

*cmb@wustl.edu
†maria.Gianfreda@le.infn.it
‡ozdemir@ese.wustl.edu
§pengb@ese.wustl.edu
¶yang@seas.wustl.edu

 

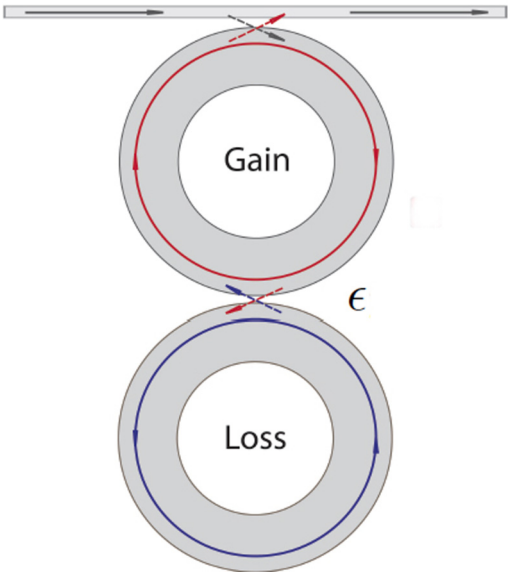


FIG. 1. (Color online) Schematic illustration of coupled $\mathcal{PT}$-symmetric whispering-gallery-mode optical microresonators. The two microresonators are directly coupled with coupling strength $\kappa$, and a tapered fiber waveguide is used to couple light in and out. The microcavity with gain (the active resonator) is a silica microtoroid doped with erbium ions. The microcavity with matched loss (the passive resonator) is also a silica microtoroid but without any dopant. The probe signal is a weak coherent light from a laser in the 1550 nm band. Gain is provided in the 1550 nm band by the erbium ions excited by a pump laser in the 1450 nm band. After it is separated from the pump using a wavelength-division-multiplexer, the output probe signal from the resonator system is monitored with a photodetector. The coupling strength $\epsilon$ between the microresonators is tuned by changing their separation by using a nanopositioning stage.

action of parity $\mathcal{P}$ is to interchange the loss and gain oscillators, and its effect is given by [25]

$$\mathcal{P}: x \to -y, \quad y \to -x, \quad p \to -q, \quad q \to -p, \tag{5}$$

while the action of time reversal $\mathcal{T}$ is to change the signs of the momenta,

$$\mathcal{T}: x \to x, \quad y \to y, \quad p \to -p, \quad q \to -q. \tag{6}$$

Note that $H$ is *not* symmetric under $\mathcal{P}$ or $\mathcal{T}$ separately, but it is symmetric under combined $\mathcal{P}$ and $\mathcal{T}$. For a one-dimensional system, $\mathcal{P}$ becomes the usual parity operator $\mathcal{P}$ : $x \to -x, p \to -p$, and $\mathcal{T}$ is the usual time-reversal operator. Because the balanced-loss-and-gain system is Hamiltonian, the energy (the value of $H$) is conserved, that is, its numerical value is constant in time. However, the expression for the energy in (4) is not recognizable as a simple sum of kinetic and potential energy (such as $p^2 + q^2 + x^2 + y^2$).

The noteworthy feature of $\mathcal{PT}$-symmetric systems with balanced loss and gain is that they exhibit phase transitions. When the coupling of the two oscillators is small, the energy flowing into the $y$ resonator cannot transfer fast enough to the $x$ resonator, where the energy is flowing out. Thus, the system cannot be in equilibrium. However, when the coupling constant $\epsilon$ exceeds a critical value, all of the energy flowing into the $y$ resonator can transfer to the $x$ resonator and the entire system can be in equilibrium. The signal that the system is in equilibrium is that the frequencies are real; complex frequencies indicate that there is exponential growth and decay.

To understand why there are phase transitions, we plot the quartic polynomial $f(\lambda)$ in (3) to see whether this polynomial cuts the horizontal axis in four places (in which case there are four real frequencies), two places (in which case there are two real frequencies and two complex frequencies), or not at all (here, there are four complex frequencies). As one can see in Fig. 2, for small values of $\epsilon$ there are no real frequencies, but as $\epsilon$ increases there is a transition at $\epsilon_1 = 2\gamma\sqrt{\omega^2 - \gamma^2}$ to a situation in which there are four real frequencies. Interestingly, one can see that when the coupling $\epsilon$ is sufficiently large, there is a second transition at $\epsilon_2 = \omega^2$. This transition is difficult to see in classical experiments because in the strong-coupling regime the loss and gain components must be so close that they overlap and therefore interfere with one another. For example, in the pendulum experiment in Ref. [13] the pendula would have to be so close that they touch and could no longer swing freely. This strong-coupling region is discussed for the case of coupled systems *without* loss and gain in Ref. [26], where it is referred to as the *ultrastrong-coupling regime*.

We conclude that the system is in equilibrium because the resonators exhibit *Rabi oscillations* (power oscillations between the two resonators) as shown in Fig. 3. Note that the Rabi oscillations are 90° out of phase.

This paper is organized as follows: In Sec. II we examine the classical solutions to (1). Next, in Sec. III we examine the quantized version of the system described by the Hamiltonian (4). We identify the quantum analogs of the $\mathcal{PT}$ phase transitions and show that the quantum and classical transitions occur at exactly the same values of the physical parameters. Finally, in Sec. IV we make some brief concluding remarks.

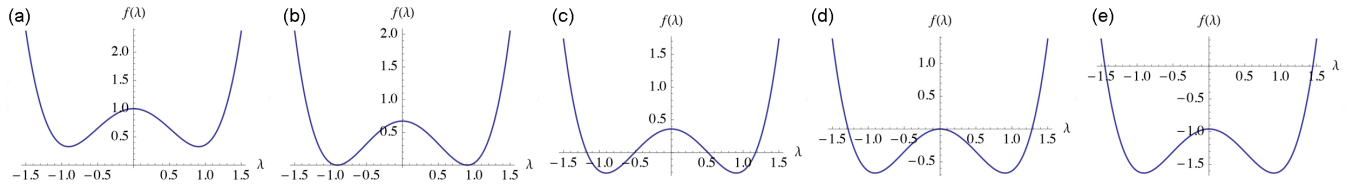


FIG. 2. (Color online) Five plots of $f(\lambda)$ in (3) for $\lambda$ in the range $-1.5 < \lambda < 1.5$. In these plots, $\omega = 1.0$, $\gamma = 0.3$, and $\epsilon$ has the values (a) $\epsilon = 0.01$ (this value of $\epsilon$ lies in the first broken-$\mathcal{PT}$ region); (b) $\epsilon = \epsilon_1 = 2\gamma\sqrt{\omega^2 - \gamma^2} \approx 0.572\,364$ (this is the first transition); (c) $\epsilon = 0.8$ (this value of $\epsilon$ lies in the unbroken-$\mathcal{PT}$ region in which the frequencies are all real); (d) $\epsilon = \epsilon_2 = \omega^2 = 1.0$ (this is the location of the second transition); and (e) $\epsilon = 1.4$ (this value of $\epsilon$ lies in the second broken $\mathcal{PT}$ region).

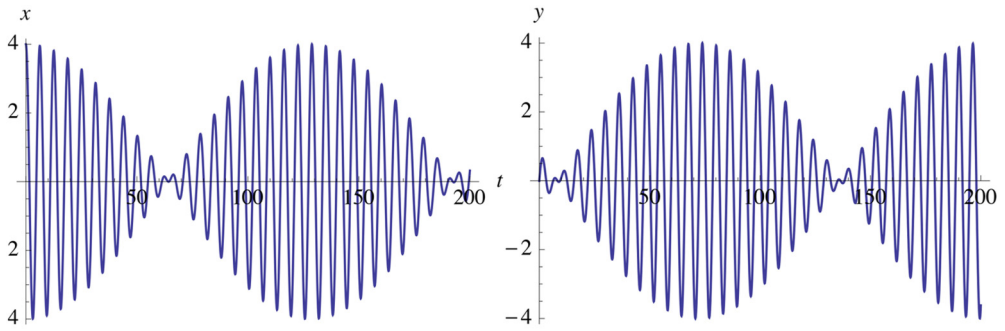


FIG. 3. (Color online) Rabi oscillations in the unbroken-$\mathcal{PT}$-symmetric region. In this figure, $\gamma = 0.01$, $\epsilon = 0.05$, and $\omega = 1.0$.

## II. CLASSICAL INTERPRETATION

### A. Balanced loss and gain

When $2\gamma = \mu = \nu$, the quartic equation (2) for $\lambda$ reduces to the biquadratic equation (3) whose solutions are

$$\lambda^2 = \omega^2 - 2\gamma^2 \pm \sqrt{\epsilon^2 - 4\gamma^2\omega^2 + 4\gamma^4}. \tag{7}$$

There are four real frequencies $\lambda$ when $\epsilon$ is in the range

$$2\gamma\sqrt{\omega^2 - \gamma^2} < \epsilon < \omega^2. \tag{8}$$

This is the unbroken classical $\mathcal{PT}$-symmetric region.

We plot the real and imaginary parts of the frequency $\lambda$ in Fig. 4 for the values $\omega = 1.0$ and $\gamma = 0.01$. For these parametric values, the $\mathcal{PT}$ phase transition occurs at $\epsilon_1 = 2\gamma\sqrt{\omega^2 - \gamma^2} \approx 0.019\,999$. When $\epsilon$ is below this critical value, the real part of $\lambda$ has one positive value, which is shown in Fig. 4, and one negative value. Also, below the critical value, the imaginary part of $\lambda$ is nonzero, as shown in Fig. 4. As $\epsilon$ approaches the critical value from below, the imaginary part of $\lambda$ vanishes and the real part of $\lambda$ bifurcates. For comparison, the experimental measurements of the real and imaginary parts of the frequencies as functions of the experimental coupling $\kappa$ are shown in Fig. 5. Note the strong resemblance of Figs. 4 and 5.

A second transition occurs when $\epsilon = \epsilon_2 = \omega^2 = 1$. Above this transition point, there is now only one supermode, as shown in Fig. 6, instead of two pairs of real frequencies.

### B. Unbalanced loss and gain

Let us consider the general case (2) in which $\mu \neq \nu$ (that is, the loss and gain are not exactly balanced). In this case, the sharp transition from a region of broken-$\mathcal{PT}$ symmetry to a region of an unbroken symmetry disappears and there is only an approximate transition [27]. To see this approximate transition, we take $\mu = 0.04$ and $\nu = 0.01$ and plot the classical frequencies $\lambda$ in Fig. 7. In contrast with Fig. 4, the frequency $\lambda$ is never exactly real. Rather, there is one region of $\epsilon$ in which the difference between the imaginary parts of the frequencies is big and the difference between the real parts of the frequencies is small but *nonzero*, and a second region in which the difference between the imaginary parts of the frequencies is small but *nonzero* and the difference between the real parts of the frequencies is big. Unlike the behavior shown in Fig. 4, at the approximate transition in Fig. 7 the real parts of the frequencies do not separate in an orthogonal direction but rather separate smoothly.

We can treat this problem perturbatively by taking $\mu$, $\nu$, and $\epsilon$ small compared with the natural frequency $\omega$. We let $\mu = \alpha\epsilon$ and $\nu = \beta\epsilon$ and expand $\lambda$ in (2) in powers of the small parameter $\epsilon$: $\lambda = \lambda_0(1 + \epsilon\lambda_1 + \epsilon^2\lambda_2 + \cdots)$. To zeroth order, $\lambda_0 = \pm i\omega$. To first order, our results are consistent with the plots in Fig. 7: For $\epsilon > (\mu + \nu)\omega$,

$$\lambda = \begin{cases} i\,\omega \pm i\,\epsilon\,\frac{\sqrt{4-(\alpha+\beta)^2\omega^2}}{4\omega} + \epsilon\,\frac{(\alpha-\beta)}{4}, \\ -i\,\omega \pm i\,\epsilon\,\frac{\sqrt{4-(\alpha+\beta)^2\omega^2}}{4\omega} + \epsilon\,\frac{(\alpha-\beta)}{4} \end{cases} \tag{9}$$

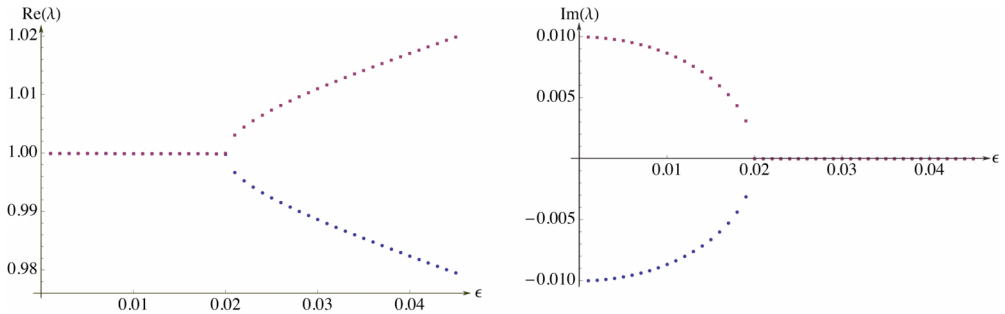


FIG. 4. (Color online) A plot of the real and imaginary parts of the classical frequency $\lambda$ in (7) for $\epsilon$ near the $\mathcal{PT}$ phase transition at $\epsilon = \epsilon_1 \approx 0.019\,999$. For this figure, $\omega = 1.0$ and $\gamma = 0.01$. Note that at the phase transition, the real and imaginary parts of the frequency bifurcate in an orthogonal direction.

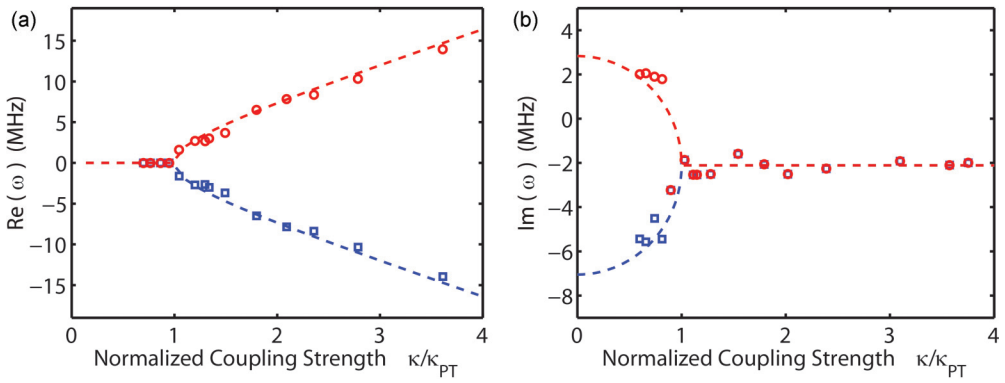


FIG. 5. (Color online) Experimental measurements of the real and imaginary parts of the eigenfrequencies of the $\mathcal{PT}$-symmetric resonators as functions of the experimental coupling strength $\kappa$. The phase transition is observed very clearly.

and for $\epsilon < (\mu+\nu)\omega$,

$$\lambda = \begin{cases} i\,\omega \pm \epsilon\frac{\sqrt{(\alpha+\beta)^2\omega^2-4}}{4\omega} + \epsilon\frac{(\alpha-\beta)}{4}, \\ -i\,\omega \pm \epsilon\frac{\sqrt{(\alpha+\beta)^2\omega^2-4}}{4\omega} + \epsilon\frac{(\alpha-\beta)}{4}. \end{cases} \tag{10}$$

## III. QUANTUM INTERPRETATION

When the loss and gain parameters in (1) are equal, the coupled oscillator system is described by the Hamiltonian $H$ in (4). To quantize this classical Hamiltonian, we replace the classical variables $p$, $q$, $x$, and $y$ with the corresponding quantum operators that satisfy the commutator equations $[x,p] = [y,q] = i$ and $[x,y] = [p,q] = [x,q] = [y,p] = 0$. In Sec. III A we discuss the eigenfunctions of $H$, and in Sec. III B we discuss the eigenvalues.

### A. Eigenfunctions of $H$

The eigenfunctions of the Hamiltonian (4) satisfy the time-independent Schrödinger equation

$$[-\partial_x\partial_y - i\gamma(y\partial_y - x\partial_x) + (\omega^2-\gamma^2)xy]\psi_{m,n}(x,y) + \frac{\epsilon}{2}(x^2+y^2)\psi_{m,n}(x,y) = E_{m,n}\psi_{m,n}(x,y). \tag{11}$$

The eigenvalues $E_{m,n}$ correspond to the eigenfunctions $\psi_{m,n}(x,y)$. The eigenfunctions have the general form

$$\psi_{m,n}(x,y) = e^{-(2axy+bx^2+cy^2)/2}P_{m,n}(x,y), \tag{12}$$

where

$$b = c^* = \frac{\epsilon}{2(a+i\gamma)} \tag{13}$$

and $a$ is a solution to the quartic equation $g(a) = 0$, where

$$g(a) = a^4 + (2\gamma^2-\omega^2)a^2 + \epsilon^2/4 + \gamma^4 - \gamma^2\omega^2. \tag{14}$$

The quantities $P_{m,n}(x,y)$ are polynomials in $x$ and $y$. The index $n$ is a non-negative integer ($n = 0,1,2,3,\ldots$) while the index $m$ is an integer that runs from 0 to $n$. Thus, the polynomials form a Pascal-like triangle in which the first index $m$ labels the row and $n$ labels the column:

$$\begin{array}{ccccccccc} & & & & P_{0,0} & & & & \\ & & & P_{1,0} & & P_{1,1} & & & \\ & & P_{2,0} & & P_{2,1} & & P_{2,2} & & \\ & P_{3,0} & & P_{3,1} & & P_{3,2} & & P_{3,3} & \\ P_{4,0} & & P_{4,1} & & P_{4,2} & & P_{4,3} & & P_{4,4} \\ \iddots & & \iddots & & \iddots & & \ddots & & \ddots \end{array}$$

In terms of the quantity

$$\Delta = \sqrt{bc-\gamma^2}, \tag{15}$$

the first seven polynomials are

$$P_{0,0} = 1,$$

$$P_{1,0} = \frac{i\gamma-\Delta}{c}x + y,$$

$$P_{1,1} = \frac{\Delta+i\gamma}{c}x + y,$$

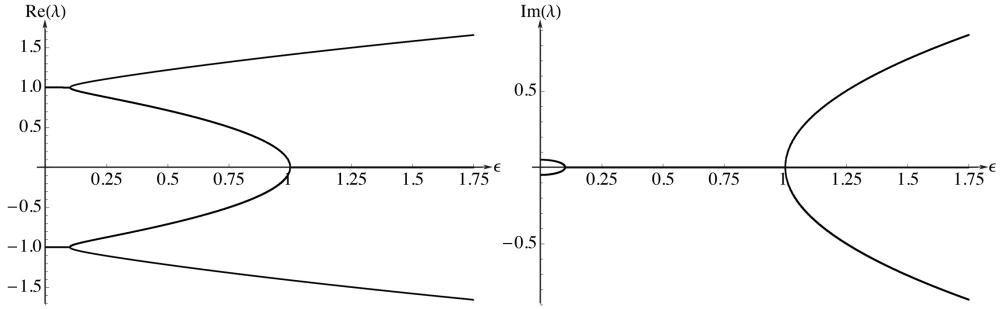


FIG. 6. A plot of the real and imaginary parts of $\lambda$ for $0 \leqslant \epsilon \leqslant 1.75$. Observe that there is a second transition at $\epsilon = \epsilon_2 = \omega^2 = 1$. For this figure, $\omega = 1.0$ and $\gamma = 0.01$.

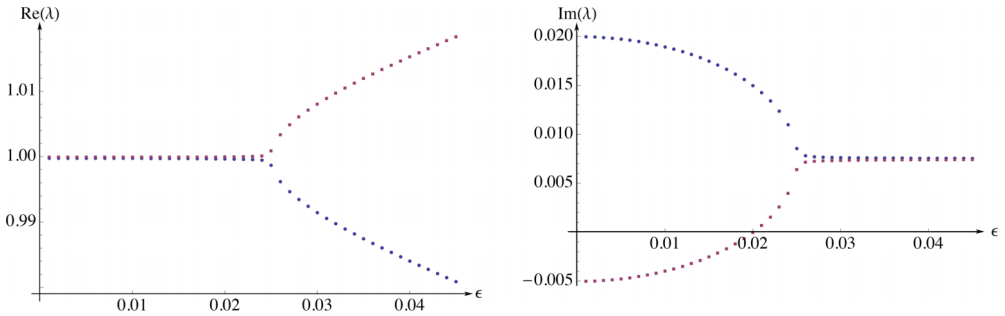


FIG. 7. (Color online) Real and imaginary parts of the classical frequencies λ for the unbalanced case in which the loss and gain parameters $\mu$ and $\nu$ are unequal. Compared with Fig. 4, the frequencies separate smoothly as a function of $\epsilon$ at the approximate transition point. For this figure, $\mu = 0.04$, $\nu = 0.01$, and $\omega = 1.0$. It is virtually impossible to have a physical system in which the loss and gain are exactly balanced, so this figure should be regarded as physically realistic while Fig. 4 is an idealization.

$$P_{2,0} = \left[\frac{(i\gamma-\Delta)x}{c} + y\right]^2 - \frac{i\gamma-\Delta}{c(a-\Delta)},$$
$$P_{2,1} = \left[\frac{i\gamma x}{c} + y\right]^2 - \frac{\Delta^2 x^2}{c^2} - \frac{i\gamma}{ac},$$
$$P_{2,2} = \left[\frac{(\Delta+i\gamma)x}{c} + y\right]^2 - \frac{\Delta+i\gamma}{c(a+\Delta)},$$
$$P_{3,0} = \left[\frac{(i\gamma-\Delta)x}{c} + y\right]^3 - \frac{3(i\gamma-\Delta)}{2c(a-\Delta)}\left[\frac{(i\gamma-\Delta)x}{c} + y\right]. \tag{16}$$

The polynomials $P_{m,n}$ satisfy two three-term recursion relations, one in the first index with the second index held fixed at 0 (at the left edge of the Pascal triangle),

$$P_{n+1,0} = \frac{(i\gamma-\Delta)x + cy}{c} P_{n,0} + \frac{n(\Delta-i\gamma)}{c(a-\Delta)} P_{n-1,0}, \tag{17}$$

and another with both indices being equal (at the right edge of the Pascal triangle),

$$P_{n+1,n+1} = \frac{(\Delta+i\gamma)x + cy}{c} P_{n,n} - \frac{n(\Delta+i\gamma)}{c(a+\Delta)} P_{n-1,n-1}. \tag{18}$$

The operators $\partial_x$ and $\partial_y$ are lowering operators for the polynomials $P_{n,0}$ and $P_{n,n}$:

$$\partial_x P_{n,0} = n\,\frac{-\Delta+i\gamma}{c} P_{n-1,0}, \quad \partial_y P_{n,0} = n\, P_{n-1,0},$$
$$\partial_x P_{n,n} = n\,\frac{\Delta+i\gamma}{c} P_{n-1,n-1}, \quad \partial_y P_{n,n} = n\, P_{n-1,n-1}. \tag{19}$$

These equations are the analogs of the relation $\partial_x H_n(x) = n H_{n-1}(x)$ for the Hermite polynomials $H_n(x)$.

Upon substituting (19) into (17) and (18), we obtain the relations

$$P_{n,0} = \frac{i\gamma-\Delta}{c}\, x\, P_{n-1,0} + y\, P_{n-1,0} + \frac{\Delta-i\gamma}{c(a-\Delta)}\,\partial_y P_{n-1,0} \tag{20}$$

and

$$P_{n,n} = \frac{\Delta+i\gamma}{c}\, x\, P_{n-1,n-1} + y\, P_{n-1,n-1} - \frac{1}{a+\Delta}\,\partial_x P_{n-1,n-1}, \tag{21}$$

from which we obtain the differential equation satisfied by the polynomials at the left and right edges of the Pascal triangle:

$$\left[\frac{(i\gamma-\Delta)x+cy}{c}\partial_y + \frac{\Delta-i\gamma}{c(a-\Delta)}\partial_y^2\right] P_{n,0} = n\, P_{n,0}, \tag{22}$$
$$\left[\frac{bx+(\Delta-i\gamma)y}{b}\partial_x + \frac{\Delta+i\gamma}{c(a-\Delta)}\partial_x^2\right] P_{n,n} = n\, P_{n,n}. \tag{23}$$

We can also construct operators that connect the polynomials on a given horizontal level in the Pascal triangle. To do this, we define the *left shift operator* **L** as

$$\mathbf{L} \equiv (y + r_1 x)\partial_y - (r_1^* y + x)\partial_x + r_2\partial_y^2 - r_2^*\partial_x^2 + r_3\partial_x\partial_y, \tag{24}$$

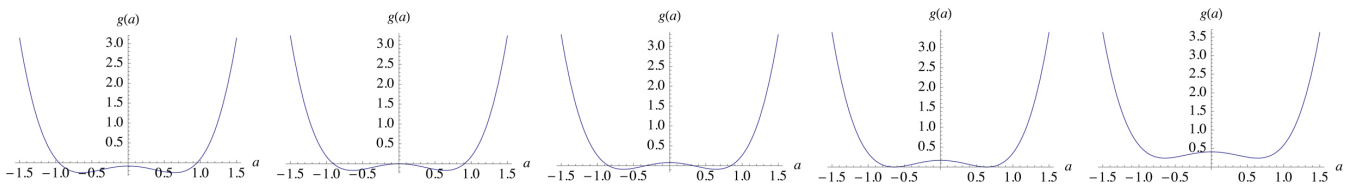


FIG. 8. (Color online) A plot of $g(a)$ in (14) for $-1.5 < a < 1.5$, $\omega = 1.0$, $\gamma = 0.3$, where (a) $\epsilon = 0.01$ (this is in the first broken region); (b) $\epsilon = \epsilon_1 = 2\gamma\sqrt{\omega^2-\gamma^2} \approx 0.572\,364$ (this is the location of the first transition); (c) $\epsilon = 0.8$ (this is in the unbroken-$\mathcal{PT}$ region in which the classical frequencies are all real); (d) $\epsilon = \epsilon_2 = \omega^2 = 1.0$ (this is the location of the second transition); and (e) $\epsilon = 1.4$ (this is in the second broken-$\mathcal{PT}$ region).

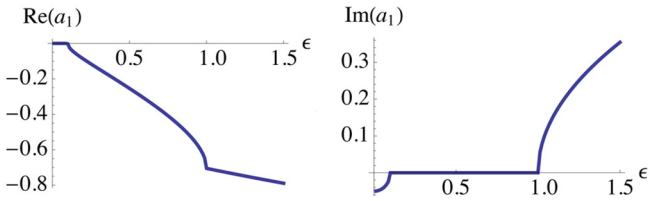


FIG. 9. (Color online) Real and imaginary parts of $a_1$ in (32) plotted as functions of $\epsilon$ for $0 \leqslant \epsilon \leqslant 1.5$. For this plot, we have taken $\gamma = 0.05$ and $\omega = 1.0$. For these values, the region of unbroken-$\mathcal{PT}$ symmetry is $0.099\,874\,9 \leqslant \epsilon \leqslant 1.0$.

where

$$r_1 = \frac{i\gamma - \Delta}{c}, \quad r_2 = \frac{(a + i\gamma)(\Delta - i\gamma)}{2ac(a - \Delta)}, \quad r_3 = \frac{i\gamma}{a(a - \Delta)}. \tag{25}$$

The effect of $\mathbf{L}$ on $P_{m,n}$ is

$$\mathbf{L}\, P_{m,n} = 2n \frac{\Delta^2 + i\Delta\gamma}{bc}\, P_{m,n-1}.$$

We also define the *right shift operator* $\mathbf{R}$ as

$$\mathbf{R} \equiv (x + s_1 y)\partial_x - (s_1^* x + y)\partial_y + s_2 \partial_x^2 - s_2^* \partial_y^2 + s_3 \partial_x \partial_y, \tag{26}$$

where

$$\begin{aligned} s_1 &= \frac{\Delta - i\gamma}{c}, \\ s_2 &= -\frac{(a - i\gamma)(\Delta - i\gamma)}{2ab(a + \Delta)}, \\ s_3 &= -\frac{i\gamma}{a(2a + \Delta)}. \end{aligned} \tag{27}$$

The effect of $\mathbf{R}$ on $P_{m,n}$ is

$$\mathbf{R}\, P_{m,n} = 2(m - n) \frac{-\Delta^2 + i\Delta\gamma}{bc}\, P_{m,n+1}.$$

Note that $P_{n,m}$ are eigenstates of the operators $\mathbf{LR}$ and $\mathbf{RL}$:

$$\mathbf{LR}\, P_{m,n} = 4(n - 1)(n - m) \frac{\Delta^2}{bc}\, P_{m,n} \tag{28}$$

for $n = 0,1,\ldots,m$, and

$$\mathbf{RL}\, P_{m,n} = 4n(n - m - 1) \frac{\Delta^2}{bc}\, P_{m,n} \tag{29}$$

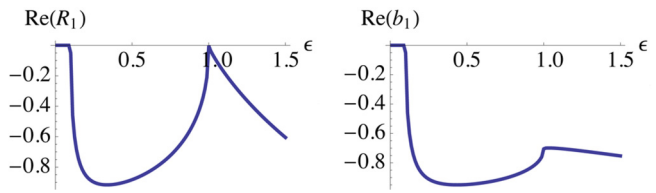


FIG. 10. (Color online) Plots of the real parts of $R_1$ and $b_1$ (the values of $R$ and $b$ corresponding to $a = a_1$) for $0 \leqslant \epsilon \leqslant 1.5$. For this plot, $\gamma = 0.05$ and $\omega = 1.0$.

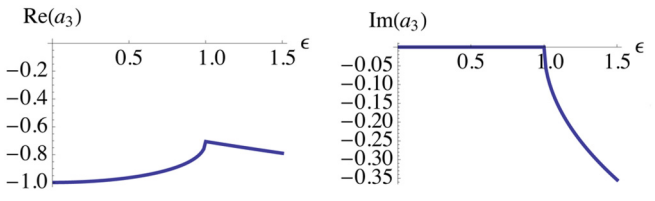


FIG. 11. (Color online) Real and imaginary parts of $a_3$ in (32) plotted as functions of $\epsilon$ for $0 \leqslant \epsilon \leqslant 1.5$. For this plot, we have taken $\gamma = 0.05$ and $\omega = 1.0$.

for $n = 0,1,\ldots,m$. If we combine (28) and (29), we obtain the interesting result

$$[\mathbf{R},\mathbf{L})\, P_{m,n} = -4m \frac{\Delta^2}{bc}\, P_{m,n}. \tag{30}$$

### B. Eigenvalues of $H$

The eigenvalues have the general form

$$E_{m,n} = (m + 1)a + (2n - m)\Delta, \tag{31}$$

where $m = 0,1,2,\ldots$ and $n = 0,1,2,\ldots,m$. Note that there are four possible spectra of eigenvalues corresponding to the four possible solutions for $a$, which are the roots of $g(a)$ in (14):

$$\begin{aligned} a_1 &= -\tfrac{1}{2}\sqrt{2\omega^2 - 4\gamma^2 - 2\sqrt{\omega^4 - \epsilon^2}}, \\ a_2 &= \tfrac{1}{2}\sqrt{2\omega^2 - 4\gamma^2 - 2\sqrt{\omega^4 - \epsilon^2}}, \\ a_3 &= -\tfrac{1}{2}\sqrt{2\omega^2 - 4\gamma^2 + 2\sqrt{\omega^4 - \epsilon^2}}, \\ a_4 &= \tfrac{1}{2}\sqrt{2\omega^2 - 4\gamma^2 + 2\sqrt{\omega^4 - \epsilon^2}}. \end{aligned} \tag{32}$$

Although there are four possible sets of eigenvalues, we will see that only two of these sets are physically acceptable; that is, there are only two sets of eigenvalues that are real and bounded below. These sets only occur in the *classical unbroken-$\mathcal{PT}$-symmetric* region of $\epsilon$ in (8).

Corresponding to the two classical phase transitions discussed earlier, there are also two quantum transitions at the same values of the coupling $\epsilon_1$ and $\epsilon_2$ as the classical transitions. To locate the quantum phase transitions, we plot in Fig. 8 the quartic polynomial $g(a)$ in (14) as a function of $a$ for various values of $\epsilon$, and we observe whether this polynomial cuts the horizontal axis in four places, two places, or not at all.

It is important to understand why there are four possible sets of quantum eigenvalues. This comes about because there are four possible pairs of Stokes wedges in the complex domain

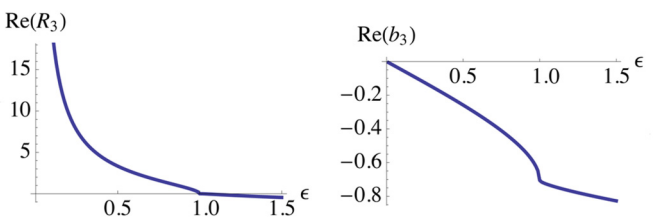


FIG. 12. (Color online) Plots of the real parts of $R_3$ and $b_3$ for $0 \leqslant \epsilon \leqslant 1.5$. For this plot, $\gamma = 0.05$ and $\omega = 1.0$.

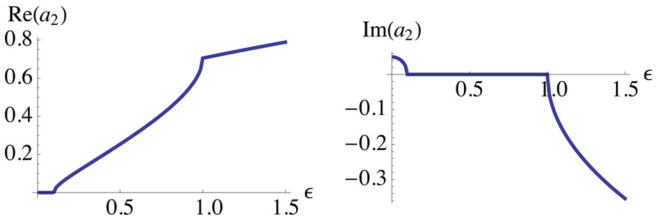


FIG. 13. (Color online) Real and imaginary parts of $a_2$ in (32) plotted as functions of $\epsilon$ for $0 \leqslant \epsilon \leqslant 1.5$. For this plot, we have taken $\gamma = 0.05$ and $\omega = 1.0$.

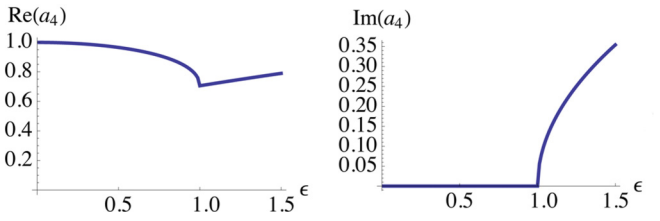


FIG. 15. (Color online) Real and imaginary parts of $a_4$ in (32) plotted as functions of $\epsilon$ for $0 \leqslant \epsilon \leqslant 1.5$. For this plot, we have taken $\gamma = 0.05$ and $\omega = 1.0$.

in which the eigenfunctions $\psi$ in (12) vanish exponentially. To explain what is going on, we use, as an elementary example, the quantum harmonic oscillator, whose Hamiltonian is $H = p^2 + x^2$. One set of eigenfunctions $\psi$ of this Hamiltonian in complex-$x$ space has the form $\psi_n(x) = e^{-x^2/2}P_n(x)$, where $P_n(x)$ is a Hermite polynomial. These eigenfunctions vanish exponentially in a pair of Stokes wedges of opening angle $\pi/2$ centered about the positive and negative real axes in the complex-$x$ plane. The eigenvalues $E_n = 2n + 1$ $(n = 0,1,2,\ldots)$ associated with these eigenfunctions are real and bounded below. There is a second set of eigenfunctions of the form $\psi_n(x) = e^{x^2/2}P_n(x)$, where $P_n(x)$ is again a Hermite polynomial. These eigenfunctions vanish exponentially in a pair of Stokes wedges of opening angle $\pi/2$ centered about the positive and negative *imaginary* axes in the complex-$x$ plane. The eigenvalues $E_n = -2n - 1$ $(n = 0,1,2,\ldots)$ associated with these eigenfunctions are real and bounded above. A full description of these two classes of eigenfunctions and eigenvalues is given in Ref. [1].

For the coupled-oscillator problem discussed in this paper, the eigenfunctions have the general form (12). The exponential component of these eigenfunctions can be rewritten as

$$e^{-(2axy+bx^2+cy^2)/2} = e^{-(bu^2+Ry^2)/2}, \tag{33}$$

where

$$u = x + ay/b \quad \text{and} \quad R = c - a^2/b. \tag{34}$$

It is important to determine the Stokes wedges in the complex-$u$ plane and in the complex-$y$ plane in which the eigenfunctions vanish. We consider each of the four values of $a$ in (32) in turn.

First, we consider $a_1$ in (32). In Fig. 9 we plot the real and imaginary parts of $a_1$ as functions of $\epsilon$ and see that $a_1$ is real in the unbroken-$\mathcal{PT}$ region (8). Furthermore, $\Delta$ in (15) is real and positive in this region. Thus, the eigenvalues in (31) are real. In the unbroken region, Re $b$ in (13) and Re $R$ in (34) are both negative (see Fig. 10). Thus, the eigenfunctions vanish exponentially in pairs of 90°-Stokes wedges centered about the imaginary axes in the $u$ and $y$ planes. However, since $a_1$ is negative, the eigenspectrum (31) is not bounded below, and thus this case must be rejected on physical grounds.

Next, we consider $a_3$ in (32). In Fig. 11, we plot $a_3$ as a function of $\epsilon$ and see that $a_3$ is real in both the first broken-$\mathcal{PT}$ region and the unbroken-$\mathcal{PT}$ region (8). Furthermore, $\Delta$ in (15) is real and positive in the unbroken region of $\epsilon$. Thus, the eigenvalues in (31) are real in the unbroken-$\mathcal{PT}$ region. In the unbroken region Re $b$ in (13) is negative and Re $R$ in (34) is positive (see Fig. 12). Thus, the eigenfunctions vanish exponentially in pairs of 90°-Stokes wedges centered about the imaginary axis in the $u$ plane and centered about the real axis in the $y$ plane. However, $a_3$ is negative, so the eigenspectrum (31) is not bounded below, and again this case must be rejected on physical grounds.

Next, we consider $a_2$ in (32). In Fig. 13, we plot $a_2$ as a function of $\epsilon$ and see that $a_2$ is real and positive in the unbroken-$\mathcal{PT}$ region (8). Again, $\Delta$ in (15) is real and positive in this region. Thus, the eigenvalues in (31) are real and positive. In the unbroken region, Re $b$ in (13) and Re $R$ in (34) are both positive (see Fig. 14). Thus, the eigenfunctions vanish exponentially in pairs of 90°-Stokes wedges centered about the real axes in both the $u$ and $y$ planes. Because the eigenspectrum (31) is bounded below and the eigenfunctions vanish exponentially in the appropriate Stokes wedges, we regard this as a physically acceptable case.

Finally, we consider $a_4$ in (32). In Fig. 15, we plot $a_4$ as a function of $\epsilon$ and see that $a_4$ is real in the first broken-$\mathcal{PT}$ region and in the unbroken-$\mathcal{PT}$ region (8). Furthermore, $\Delta$ in (15) is real and positive in the unbroken-$\mathcal{PT}$ region. Thus, the eigenvalues in (31) are real. In the unbroken region, Re $b$ in (13) is positive and Re $R$ in (34) is negative (see Fig. 16). Thus, the eigenfunctions vanish exponentially in pairs of 90°-Stokes wedges centered about the real axis in the $u$ plane and centered about the imaginary axis in the $y$ plane. Because $a_4$ is positive,

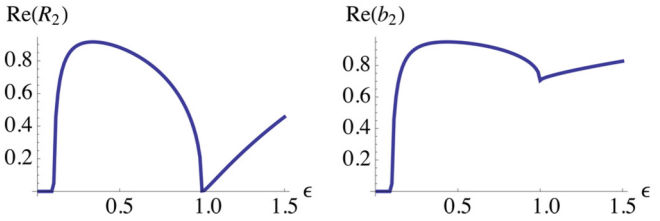


FIG. 14. (Color online) Plots of the real parts of $R_2$ and $b_2$ for $0 \leqslant \epsilon \leqslant 1.5$. For this plot, $\gamma = 0.05$ and $\omega = 1.0$.

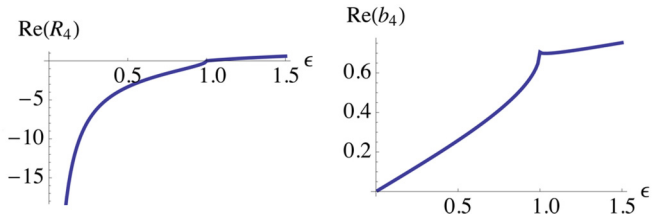


FIG. 16. (Color online) Plots of the real parts of $R_4$ and $b_4$ for $0 \leqslant \epsilon \leqslant 1.5$. For this plot, $\gamma = 0.05$ and $\omega = 1.0$.

the eigenspectrum (31) is bounded below, and because the eigenfunctions vanish exponentially in the appropriate Stokes wedges in the $u$ and $y$ planes, we again regard this case as physically acceptable.

It is interesting but perhaps not surprising that the Hamiltonian (4) has two distinct physically allowed positive spectra, which correspond to the choices $a = a_2$ and $a = a_4$. It is not surprising that in the context of $\mathcal{PT}$ quantum mechanics, one Hamiltonian can have two independent positive spectra. This phenomenon was discussed previously for the case of the sextic quantum-mechanical Hamiltonian $H = p^2 + x^6$ in Ref. [28]. This sextic Hamiltonian also has two positive spectra, which are associated with two distinct pairs of Stokes wedges in which the eigenfunctions vanish exponentially.

## IV. CONCLUDING REMARKS

In this paper, we have studied the behavior of a system of two coupled oscillators, one with gain and the other with loss. If the gain and loss parameters are equal, the system is $\mathcal{PT}$-symmetric. Furthermore, it is described by a Hamiltonian and thus the energy is exactly conserved. Both the classical and the quantum systems exhibit two transitions at exactly the same values of the coupling parameter, $\epsilon = \epsilon_1$ and $\epsilon = \epsilon_2$.

Specifically, if the coupling is smaller than the critical value $\epsilon_1$, the system is not in equilibrium even though the energy is conserved. At the classical level, the lack of equilibrium manifests itself as complex frequencies and exponentially growing and decaying modes; at the quantum level, the lack of equilibrium is associated with complex energy levels. Above the critical value $\epsilon_1$, the system is in an unbroken-$\mathcal{PT}$-symmetric phase; at the classical level, the system is in equilibrium and the oscillators exhibit Rabi oscillations; and at the quantum level, the system exhibits not one but two independent sets of real spectra and associated eigenfunctions.

There is also a second transition point $\epsilon_2$ above which the system is no longer in equilibrium and the quantum energy levels become complex. This superstrong-coupling regime is very hard to study at the classical experimental level because it requires that the oscillators be strongly coupled, so much so that they are likely to interfere with one another. However, at the quantum level it might be possible to perform experiments using quantum optics techniques that can actually observe the second phase transition. Such quantum experiments might also prove to be extremely interesting because they may provide a platform upon which to study quantum entanglement [26].

In future work, we will study systems of more than two coupled oscillators. The phase structure of such systems is interesting; we have found that as the number of coupled oscillators increases, there are more and more phase transition points.

## ACKNOWLEDGMENTS

M.G. is grateful for the hospitality of the Department of Physics at Washington University. C.M.B. thanks the U.S. Department of Energy and M.G. thanks the INFN (Lecce) for financial support. L.Y. acknowledges the support from ARO Grant No. W911NF-12-1-0026.

[1] C. M. Bender, Rep. Prog. Phys. **70**, 947 (2007).
[2] A. Mostafazadeh, J. Geom. Methods Mod. Phys. **7**, 1191 (2010).
[3] J. Rubinstein, P. Sternberg, and Q. Ma, Phys. Rev. Lett. **99**, 167003 (2007).
[4] N. M. Chtchelkatchev, A. A. Golubov, T. I. Baturina, and V. M. Vinokur, Phys. Rev. Lett. **109**, 150405 (2012).
[5] A. Guo, G. J. Salamo, D. Duchesne, R. Morandotti, M. Volatier-Ravat, V. Aimez, G. A. Siviloglou, and D. N. Christodoulides, Phys. Rev. Lett. **103**, 093902 (2009).
[6] C. E. Rüter, K. G. Makris, R. El-Ganainy, D. N. Christodoulides, M. Segev, and D. Kip, Nature Phys. **6**, 192 (2010).
[7] Z. Lin, H. Ramezani, T. Eichelkraut, T. Kottos, H. Cao, and D. N. Christodoulides, Phys. Rev. Lett. **106**, 213901 (2011).
[8] L. Feng, M. Ayache, J. Huang, Y.-L. Xu, M. H. Lu, Y. F. Chen, Y. Fainman, and A. Scherer, Science **333**, 729 (2011).
[9] S. Bittner, B. Dietz, U. Günther, H. L. Harney, M. Miski-Oglu, A. Richter, and F. Schäfer, Phys. Rev. Lett. **108**, 024101 (2012).
[10] K. F. Zhao, M. Schaden, and Z. Wu, Phys. Rev. A **81**, 042903 (2010).
[11] C. Zheng, L. Hao, and G. L. Long, Philos. Trans. R. Soc. A **371**, 20120053 (2013).
[12] J. Schindler, A. Li, M. C. Zheng, F. M. Ellis, and T. Kottos, Phys. Rev. A **84**, 040101(R) (2011).
[13] C. M. Bender, B. Berntson, D. Parker, and E. Samuel, Am. J. Phys. **81**, 173 (2013).
[14] B. Peng, S. K. Özdemir, F. Lei, F. Monifi, M. Gianfreda, G. L. Long, S. Fan, F. Nori, C. M. Bender, and L. Yang, arXiv:1308.4564. This work was reported in the conference "Pseudo-Hermitian Hamiltonians in Quantum Physics 12," Istanbul, Turkey, July 2013.
[15] The structure of the Hamiltonian (4) is quite similar to that of the Pais-Uhlenbeck Hamiltonian studied in C. M. Bender and P. D. Mannheim, Phys. Rev. Lett. **100**, 110402 (2008).
[16] H. Bateman, Phys. Rev. **38**, 815 (1931).
[17] P. M. Morse and H. Feshbach, *Methods of Theoretical Physics* (McGraw-Hill, New York, 1953), Vol. I.
[18] F. Bopp, Sitz.-Bcr. Bayer. Akad. Wiss. Math.-naturw. KI. **67** (1973).
[19] H. Feshbach and Y. Tikochinsky, in *A. Festschrift for I. I. Rabi* [Trans. N.Y. Acad. Sci., Ser. 2 **38**, 44 (1977)].
[20] Y. Tikochinsky, J. Math. Phys. **19**, 888 (1978).
[21] H. Dekker, Phys. Rep. **80**, 1 (1981).
[22] E. Celeghini, M. Rasetti, and G. Vitiello, Ann. Phys. (N.Y.) **215**, 156 (1992).
[23] R. Banerjee and P. Mukherjee, J. Phys. A **35**, 5591 (2002).
[24] D. Chruściński and J. Jurkowski, Ann. Phys. (N.Y.) **321**, 854 (2006).
[25] The minus sign in (5) is optional; it is included so that this definition of parity reduces to the conventional one for the case of just one oscillator.
[26] V. Sudhir, M. G. Genoni, J. Lee, and M. S. Kim, Phys. Rev. A **86**, 012316 (2012).
[27] The case of an approximate $\mathcal{PT}$ transition (that is, a smooth bifurcation) is also considered in H. Benisty, C. Yan, A. Degiron, and A. T. Lupu, J. Lightwave Technol. **30**, 2675 (2012).
[28] C. M. Bender and S. P. Klevansky, Phys. Rev. Lett. **105**, 031601 (2010).